JPE 16-5-27

http://dx.doi.org/10.6113/JPE.2016.16.5.1884
ISSN(Print): 1598-2092 / ISSN(Online): 2093-4718

A Calculation Method for the Nonlinear Crowbar Circuit of DFIG Wind Generation based on Frequency Domain Analysis

Hao Luo†, Mingyao Lin*, Yang Cao**, Wei Guo**, Li Hao*, and Peng Wang***

†,***School of Electric Power Engineering, Nanjing Institute of Technology, Nanjing, China
*School of Electrical Engineering, Southeast University, Nanjing, China
**Guodian Nanjing Automation Co., Ltd, Nanjing, China

Abstract

The ride-through control of a doubly-fed induction generator (DFIG) for the voltage sags on wind farms utilizing crowbar circuits by which the rotor side converter (RSC) is disabled has being reported in many literatures. An analysis and calculation of the transient current when the RSC is switched off are of significance for carrying out the low voltage ride through (LVRT) of a DFIG. The mathematical derivation is highlighted in this paper. The zero-state and zero-input responses of the transient current in the frequency domain through a Laplace transformation are investigated, and the transient components in the time domain are achieved. With the characteristics worked out from the linear resolving without modeling simplification, the selection of the resistance in the linear crowbar circuit and the value conversion from a linear circuit to a nonlinear one is proposed to setup the attenuation rate. In terms of grid code requirements, the theoretical analysis for the time constant of the transient components attenuation insures the controllability when the excitation of the RSC is resumed and it guarantees the reserved time for the response of the reactive power compensation. Simulations are executed in MATLAB/SIMPOWER and experiments are carried out to validate the theoretical analysis. They indicate that the calculation method is effective for selection of the resistance in a crowbar circuit for LVRT operations.

Key words: Crowbar, Doubly-fed induction generator, Laplace transformation, Voltage sags

NOMENCLATURE

U_r^r, U_r^s	Rotor voltage in the rotor and stator reference frames
U_s^s	Stator voltage in the stator reference frame
I_s^s, I_r^s	Stator and rotor current in the stator reference frame
I_s^r, I_r^r	Stator and rotor current in the rotor reference frame
ψ_s^s, ψ_r^s	Stator and rotor fluxes in the stator reference frame
R_s, R_r	Resistances of the stator and rotor
$L_{s\sigma}, L_{r\sigma}$	Leakage inductances of the stator and rotor
L_m, L_s, L_r	Mutual inductances, stator and rotor inductances
ω_1, ω_r	Synchronous and rotor electrical angular speeds
U_{dc}	DC-LINK voltage of the back to back converter
p_n	Number of pole-pairs
k	Winding conversion coefficient

Superscripts

$\rightarrow$	Space vectors
s, r	Stator and rotor reference frames
'	Values after the winding conversion

Subscripts

α, β	Stationary α-axis and β-axis
s, r	Stator and rotor
cal	Calculated result
sim	Simulated result

Manuscript received Feb. 1, 2016; accepted Jun. 9, 2016
Recommended for publication by Associate Editor Dong-Myung Lee.
†Corresponding Author: luohao@njit.edu.cn
Tel: +86-025-86118400, Fax: +86-025-86118400, Nanjing Institute of Technology
*School of Electrical Engineering, Southeast University, China
**Guodian Nanjing Automation Co., Ltd., China
***School of Electric Power Eng., Nanjing Institute of Technology, China

ex Experimental result
Boldface Variables in the frequency domain

I. INTRODUCTION

Many wind farms employ wind turbines based on DFIG systems, where the converter is typically rated at around 30% of the system's rated capacity. However, the rated slip power of the converter results in damage to the back-to-back converter when a grid voltage sag happens. The induced high voltage at the rotor side and the transient attenuating current through the rotor winding result in imbalances of the energy stream, which leads to voltage fluctuations of the DC-LINK, the high electromagnetic torque ripples, etc. Due to the existence of the transient flux components in the winding, it needs higher output voltage with different frequency to keep the rotor current under control, which exceeds the maximum voltage output of the RSC attributing to the DC-LINK.

Several types of LVRT technologies for DFIG wind turbine systems are summarized and evaluated respectively in [1]. The application of a crowbar circuit is a prevalent way to assimilate transient energy at the rotor side. The maximum short circuit current is analyzed in the time domain for a crowbar-protected DFIG during LVRT [2]. In [3], a short circuit of the rotor winding is simulated when the DC-link clamp effect occurs. A flowchart of the crowbar circuit control is proposed in [4]. To avoid over-voltage after a crowbar circuit is triggered, a principle of selecting the crowbar resistance is given by [5]. In [6], the flux response of a DFIG is researched with the crowbar as a linear circuit. One kind of adjustable resistance crowbar structure is proposed in reference [7]. The turn-on and turn-off strategy of the crowbar circuit is achieved depending on the DC-LINK voltage and the time constant of the damping of the DC component in the stator [8]. The rotor current and DC-LINK voltage are applied as criteria to optimize the crowbar resistance in [9]. Optimizing the resistance value of a crowbar circuit based on the Analytic Hierarchy Process (AHP) while taking into account its effects on the reactive power, rotor current, voltage and electromagnetic torque is proposed in [10].

Although many important articles have been published to investigate the bypass effect of crowbar circuits and the control logic, some difficulties still exist in the analytic expression of the transient current and flux linkage. In [11], the transient characteristics are analyzed and calculated under voltage dips when the rotor is assumed to be an open circuit, whereas the resolution of the transient components is not realized when the rotor current is not zero.

In [2], [6] and [12]-[15]，the transient time constants of the stator and rotor are applied to resolve the transient behavior of the current and flux. However, a theoretical analysis by using the transient time constant as the attenuation time constant is not given, and the results of the resolutions reported in these papers are not identical. A short circuit current analysis of the DFIG is realized by solving the state space equation [16]. However, due to the convenience of resolving the matrix function, approximations and simplifications are made.

The physical transient behavior of the DFIG when there are grid voltage sags or swells in specific proportions is a hotspot and difficulty. The engineering design of the crowbar circuit is still based on experience. Furthermore, researchers are addressing this issue by assuming a linear crowbar circuit, whereas a nonlinear rectifier is utilized. Consequently the parameters of the crowbar need a lot of adjustment in engineering applications based on the trial method or simulations.

Due to the indefinite physical meaning of the transient course, simulations runs short of significance for investigating the effect of varying the crowbar resistance and DFIG parameters on the dynamic performance.

Concerning the resolving method based on the references, all of the models are approximate. In order to get an accurate expression of the LVRT response when the crowbar circuit is fired while keeping the conciseness of the results, a modeling method based on the Laplace transformation is proposed in this paper. It can be regarded as a rigorous mathematical method neglecting only the non-linear factors including the nonlinear excitation, skin effect, slot effect, etc.

The present paper extends the previous studies. Hereafter, the transient current and flux linkage are calculated by Laplace transformations and inverse transformations in both the frequency and time domains. As demonstrated in this paper, the attenuation characteristics of the transient components after the crowbar is fired depend on the crowbar resistance and rotation speed of the rotor. In an effort to satisfy grid code requirements, the selection strategy of the crowbar resistance is applied according to the proposed approach to guarantee the attenuation rate of the transient components, the reserved response time of the reactive power compensation and the controllability when excitation of the RSC is resumed. Concerning the setting of the crowbar resistance, an approximate linear calculation approach for nonlinear circuits is proposed.

Rigorous mathematical derivation is proposed in this paper, which is of great importance to the design of the crowbar resistance, and the dynamic behavior of a DFIG is analyzed during grid disturbances using active crowbar protection. This paper is organized as follows. In Section II, the analytic expressions of the transient current are proposed. In section III, the principle of selecting the crowbar resistor is discussed. The impedance of each transient fundamental component is derived for the nonlinear circuit in Section IV. A validated model is used in Section V to evaluate the crowbar performance with respect to the calculated crowbar resistance. Experimental results are shown in Section VI, and some conclusions are

summarized in Section VII.

II. Resolving of the Transient Current during Voltage Sags

The rotor voltage vector equation in the static reference frame of the rotor is expressed as:

$$\vec{U}_r^{r'} = R_r' \vec{I}_r^{r'} + L_{rr}' \frac{d\vec{I}_r^{r'}}{dt} + L_{r\delta}' \frac{d\vec{I}_r^{r'}}{dt} + L_m' \frac{d\vec{I}_s^{r'}}{dt} \quad (1)$$

where L_{rr}' is the mutual-induction of the rotor phase winding.

After winding conversion, L_{rr}' is equal to L_m'. Then (1) can be calculated as:

$$\vec{U}_r^{r'} = R_r' \vec{I}_r^{r'} + L_m' \left(\frac{d\vec{I}_r^{r'}}{dt} + \frac{d\vec{I}_s^{r}}{dt}\right) + L_{r\delta}' \frac{d\vec{I}_r^{r'}}{dt} \quad (2)$$

In the stationary reference frame of the stator, (2) can be represented as:

$$\vec{U}_r^{s'} = R_r' \vec{I}_r^{s'} + L_r' \frac{d\vec{I}_r^{s'}}{dt} + L_m' \frac{d\vec{I}_s^{s}}{dt} - j\omega_r L_m' \vec{I}_s^{s} - j\omega_r L_r' \vec{I}_r^{s'} \quad (3)$$

where θ_r is the angle between phase A of the stator winding and the rotor winding. Due to heavy moment inertia, the rotating speed during a voltage sag is assumed to be constant, i.e., $d\theta_r / dt$ is equal to ω_r which is constant during a voltage sag.

Considering the initial values, the Laplace transformation of (3) can be derived as follows:

$$\boldsymbol{I}_r^{s'} = \frac{\boldsymbol{U}_r^{s'} + L_r' \vec{I}_r^{s'}(t_0) + L_m' \vec{I}_s^{s}(t_0) - (s - j\omega_r) L_m' \boldsymbol{I}_s^{s}}{R_r' + (s - j\omega_r) L_r'} \quad (4)$$

The following equation is obtained by substituting (4) into $\boldsymbol{\psi}_s^s = L_s \boldsymbol{I}_s^s + L_m' \boldsymbol{I}_r^{s'}$:

$$\boldsymbol{\psi}_s^s = L_s \boldsymbol{I}_s^s + L_m' \left[\frac{\boldsymbol{U}_r^{s'} + L_r' \vec{I}_r^{s'}(t_0) + L_m' \vec{I}_s^{s}(t_0) - (s - j\omega_r) L_m' \boldsymbol{I}_s^{s}}{R_r' + (s - j\omega_r) L_r'}\right] \quad (5)$$

Considering the initial value of the flux, the Laplace transformation of the stator voltage vector equation in the stator reference frame is:

$$\boldsymbol{U}_s^s = R_s \boldsymbol{I}_s^s + s\boldsymbol{\psi}_s^s - \vec{\psi}_s^s(t_0) \quad (6)$$

The expression of the stator voltage in the frequency domain is:

$$\boldsymbol{U}_s^s = \frac{|U_{spm}|}{s - j\omega_1} e^{j\theta_{sp0}} + \frac{|U_{snm}|}{s + j\omega_1} e^{j\theta_{sn0}} \quad (7)$$

where θ_{sp0} and θ_{sn0} are the initial phase angles of the voltage in the positive and negative sequences, respectively.

Considering a short circuit of the rotor through the crowbar circuit ($U_r^{s'}$=0), the stator current, stator flux linkage, rotor current and rotor flux linkage can be composed of the zero-state response and the zero-input response whether the grid voltage fault is symmetrical or asymmetrical [17].

A. Solution of the Stator Current

Substituting (5) and (7) into (6) can calculate I_s^s in the frequency domain as follows:

$$\boldsymbol{I}_s^s = \boldsymbol{I}_{s1}^s + \boldsymbol{I}_{s2}^s \quad (8)$$

where $\boldsymbol{I}_{s1}^s$ is the zero-state response and $\boldsymbol{I}_{s2}^s$ is the zero-input response, which can be expressed as (9) and (10):

$$\boldsymbol{I}_{s1}^s = \frac{NUM_1(s)}{DEN_1(s)} = \frac{B_1(s + j\omega_1)|U_{spm}|e^{j\theta_{sp0}} + B_1(s - j\omega_1)|U_{snm}|e^{j\theta_{sn0}}}{(s^2 + \omega_1^2)A_1} \quad (9)$$

$$\boldsymbol{I}_{s2}^s = \frac{NUM_2(s)}{DEN_2(s)} = \frac{B_1 \vec{\psi}_s^s(t_0) - sL_m' \vec{\psi}_r^{s'}(t_0)}{A_1} \quad (10)$$

Where:

$A_1 = s^2(L_r'L_s - L_m'^2) + s(L_r'R_s + R_r'L_s - j\omega_r L_r'L_s + j\omega_r L_m'^2)$
$- j\omega_r L_r'R_s + R_r'R_s$ and $B_1 = R_r' + (s - j\omega_r)L_r'$.

The four poles of $NUM_1(s) / DEN_1(s)$ are:

$$\begin{cases} a_1 = j\omega_1 \\ a_2 = -j\omega_1 \\ a_3 = \dfrac{C_1 + \sqrt{E_1}}{D_1} \\ a_4 = \dfrac{C_1 - \sqrt{E_1}}{D_1} \end{cases} \quad (11)$$

where $C_1 = -R_s L_r' - R_r' L_s + L_s L_r' j\omega_r - j\omega_r L_m'^2$, $D_1 = 2(L_s L_r' - L_m'^2)$ and $E_1 = C_1^2 - 2D_1(R_s R_r' - j\omega_r R_s L_r')$.

Furthermore the two poles of $NUM_2(s) / DEN_2(s)$ are:

$$\begin{cases} b_1 = a_3 \\ b_2 = a_4 \end{cases} \quad (12)$$

According to (11) and (12), the attenuation time constants of the zero-state and the zero-input responses are equal to each other for the stator current. With the above poles and the derivatives of $DEN_1(s)$ and $DEN_2(s)$, which are $dDEN_1(a_n)/ds$ and $dDEN_2(b_n)/ds$, the stator current in the time domain is calculated through the inverse Laplace transformation :

$$i_s(t) = \sum_{n=1,2,3,4} \frac{NUM_1(a_n)}{dDEN_1(a_n)/ds} e^{a_n t} + \sum_{n=1,2} \frac{NUM_2(b_n)}{dDEN_2(b_n)/ds} e^{b_n t} \quad (13)$$

Consider that $\mathrm{Re}(a_1) = \mathrm{Re}(a_2)$ =0. Meanwhile, the values of $\mathrm{Re}(a_3)$, $\mathrm{Re}(a_4)$, $\mathrm{Re}(b_1)$ and $\mathrm{Re}(b_2)$ are not zero. Therefore, the steady state and transient components of the stator current are described as (14) and (15):

$$\vec{i}_s(t)|_{t\to\infty} = \sum_{n=1,2} \frac{NUM_1(a_n)}{dDEN_1(a_n)/ds} e^{a_n t} \quad (14)$$

$$\vec{i}_{s\_transient}(t) = \sum_{n=3,4} \frac{NUM_1(a_n)}{dDEN_1(a_n)/ds} e^{a_n t} + \sum_{n=1,2} \frac{NUM_2(b_n)}{dDEN_2(b_n)/ds} e^{b_n t} \quad (15)$$

In (15), the value of $-1/\mathrm{Re}(a_3)$, $-1/\mathrm{Re}(a_4)$, $-1/\mathrm{Re}(b_1)$ and $-1/\mathrm{Re}(b_2)$ is the attenuation time constant of each transient component[17].

B. Solution of the Rotor Current

The rotor current in the frequency domain can be expressed by substituting $\boldsymbol{I}_{s1}^{s}$ and $\boldsymbol{I}_{s2}^{s}$ into (4):

$$\boldsymbol{I}_{r1}^{s'}=\frac{NUM_3(s)}{DEN_3(s)}=-\frac{(s-j\omega_r)L_m^{'}}{B_1}\boldsymbol{I}_{s1}^{s} \tag{16}$$

$$\boldsymbol{I}_{r2}^{s'}=\frac{NUM_4(s)}{DEN_4(s)}=\frac{\vec{\psi}_r^{s'}(t_0)}{B_1}-\frac{(s-j\omega_r)L_m^{'}}{B_1}\boldsymbol{I}_{s2}^{s} \tag{17}$$

where $\boldsymbol{I}_{r1}^{s'}$ is the zero-state response and $\boldsymbol{I}_{r2}^{s'}$ is the zero-input response of the rotor current. The corresponding expressions are given in detail in Appendix A.

The four poles of $NUM_3(s)/DEN_3(s)$ and the three poles of $NUM_4(s)/DEN_4(s)$ are expressed by (18) and (19):

$$\begin{cases} c_1=a_1 \\ c_2=a_2 \\ c_3=a_3 \\ c_4=a_4 \end{cases} \tag{18}$$

$$\begin{cases} d_1=-(R_r^{'}/L_r^{'})+j\omega_r \\ d_2=a_3 \\ d_3=a_4 \end{cases} \tag{19}$$

With the poles and the derivatives of $DEN_3(s)$ and $DEN_4(s)$, the rotor current in the time domain is calculated by the inverse Laplace transformation:

$$\vec{i}_r^{s'}(t)=\sum_{n=1,2,3,4}\frac{NUM_3(c_n)}{dDEN_3(c_n)/ds}e^{c_n t}+\sum_{n=1,2,3}\frac{NUM_4(d_n)}{dDEN_4(d_n)/ds}e^{d_n t} \tag{20}$$

On account of the zero value of $\mathrm{Re}(c_1)$ and $\mathrm{Re}(c_2)$, the steady state current and the transient component of the rotor are described by (21) and (22):

$$\vec{i}_r^{s'}(t)|_{t\to\infty}=\sum_{n=1,2}\frac{NUM_3(c_n)}{dDEN_3(c_n)/ds}e^{c_n t} \tag{21}$$

$$\begin{aligned} \vec{i}_{r\_transient}^{s'}(t)=&\sum_{n=3,4}\frac{NUM_3(c_n)}{dDEN_3(c_n)/ds}e^{c_n t} \\ &+\sum_{n=1,2,3}\frac{NUM_4(d_n)}{dDEN_4(d_n)/ds}e^{d_n t} \end{aligned} \tag{22}$$

In (22), the value of $-1/\mathrm{Re}(c_3)$, $-1/\mathrm{Re}(c_4)$, $-1/\mathrm{Re}(d_1)$, $-1/\mathrm{Re}(d_2)$ and $-1/\mathrm{Re}(d_3)$ is the time constant of the attenuation for each transient component.

III. Selection of Crowbar Resistor for the Linear Circuit

The characteristics of the transient current are researched in this section based on a 690V/30kW laboratory DFIG test rig. The attenuation rate of the transient current depends on the real parts of a_3, a_4 and d_1, which are the function of ω_r and $R_r^{'}$ shown in Fig.1 and Fig.2. The resolving is based on the parameters listed in Appendix B. The resistance of the rotor winding (after the winding conversion) is equal to 0.3226Ω, and the resistance (after the winding conversion) of the linear crowbar circuit is adjusted from 0Ω to 1.2774Ω. With the expression of $\boldsymbol{I}_{r2}^{s'}$, given in Appendix A, $\frac{NUM_4(d_1)}{dDEN_4(d_1)/ds}|_{s=d_1}$ approaches zero while $0.7\omega_1\le\omega_r\le1.3\omega_1$. Therefore, it is clear that the attenuation of $\frac{NUM_4(d_1)}{dDEN_4(d_1)/ds}e^{j\,\mathrm{Im}(d_1)t}$ can be omitted.

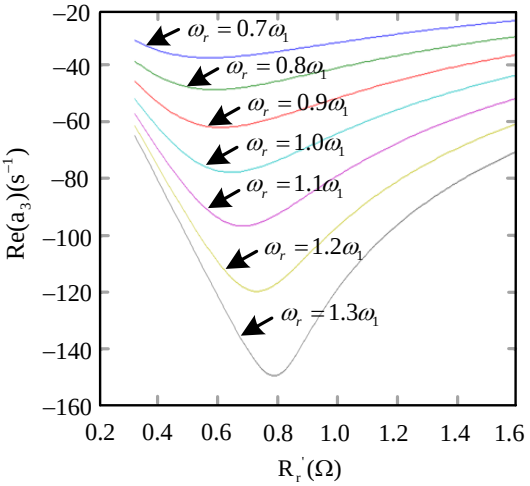

Fig. 1. Curves of $\mathrm{Re}(a_3)$.

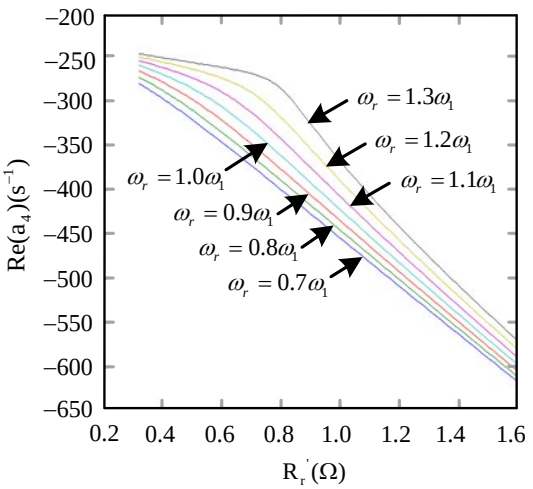

Fig. 2. Curves of $\mathrm{Re}(a_4)$.

Since $0>\mathrm{Re}(a_3)\gg\mathrm{Re}(a_4)$, it can be concluded that the attenuation rates of the transient components of either the stator or the rotor current mainly lie on $\mathrm{Re}(a_3)$. From Fig.1, it can be seen that as long as the attenuation rate can be guaranteed when the DFIG runs at the highest positive slip, the crowbar circuit can insure a higher attenuation rate for the transient components at a higher rotating speed.

According to the response time of the reactive power

compensation required by grid codes in China, which is 75ms after voltage sags, the time duration of the crowbar conducting state is set up to 40ms in this paper. It can be seen from Fig. 1 that $d\,\mathrm{Re}(a_3)/dR_r^{'}|_{R_r^{'}=0.5333}=0$ if ω_r is equal to the lowest bound of the slip. The attenuation ratio in 40ms when $R_r^{'}=0.5333$ is given by:

$$\sigma_{opt}=e^{\mathrm{Re}(a_3)|_{R_r^{'}=0.5333}\times 0.04}=23.97\% \quad (23)$$

According to the rotor resistance $0.3226\,\Omega$ after the winding conversion listed in Appendix B, the optimal resistor in the linear crowbar circuit is calculated by the winding conversion as follows:

$$R_{c\_linear\_opt}=(0.5333-0.3226)\times k^2\approx 3.3(\Omega) \quad (24)$$

IV. Analysis of the Fundamental Wave Component for a Nonlinear Crowbar

Assuming that the crowbar resistor $R_{c\_linear}^{'}$ in the linear circuit was applied, the voltage drop of the crowbar resistance can be expressed as (25):

$$\begin{aligned}\vec{E}_{crowbar\_linear}^{'}&=R_{c\_linear}^{'}\sum_{n=1,2,3,4}\frac{NUM_3(c_n)}{dDEN_3(c_n)/ds}e^{c_nt}\\&+R_{c\_linear}^{'}\sum_{n=1,2,3}\frac{NUM_4(d_n)}{dDEN_4(d_n)/ds}e^{d_nt}\end{aligned} \quad (25)$$

Considering the application of a nonlinear crowbar circuit based on the uncontrolled rectifier and $R_{c\_nonlinear}^{'}$, the rotor current can be written as:

$$\begin{aligned}\vec{i}_{r\_transient}^{s'}(t)&=\frac{R_{c\_nonlinear}^{'}}{\sqrt{3v_1^2+3w_1^2}}\sum_{n=1,2,3,4}\frac{NUM_3(c_n)}{dDEN_3(c_n)/ds}e^{c_nt}\\&+\frac{R_{c\_nonlinear}^{'}}{\sqrt{3v_1^2+3w_1^2}}\sum_{n=1,2,3}\frac{NUM_4(d_n)}{dDEN_4(d_n)/ds}e^{d_nt}\\&+\sum_{n=1,2,3,4}\sum_{h=1}^{\infty}f_n(\mathrm{Im}(hc_n))+\sum_{n=1,2,3}\sum_{h=1}^{\infty}g_n(\mathrm{Im}(hd_n))\end{aligned} \quad (26)$$

where $v_1=\frac{3}{4\pi}+\frac{\sqrt{3}}{6}$ and $w_1=\frac{1}{2}+\frac{3\sqrt{3}}{4\pi}$, f_n and g_n are functions of the extra harmonic current caused by the zero-state and the zero-input responses, and h is the harmonic order.

Due to the impedance of the "fundamental" components whose angle speeds depend on $\mathrm{Im}(c_n)$ and $\mathrm{Im}(d_n)$, once the value of $R_{c\_linear}^{'}$ is worked out through a linear calculation, $R_{c\_nonlinear}^{'}$ can be given with the winding conversion applied in the nonlinear circuit:

$$R_{c\_nonlinear}^{'}=R_{c\_linear}^{'}\sqrt{3v_1^2+3w_1^2} \quad (27)$$

Based on this principle, all of the extra harmonic components caused by the nonlinear circuit, whose angle speed is different with $\mathrm{Im}(c_n)$ and $\mathrm{Im}(d_n)$, are omitted.

V. Simulation Results

For verifying the above theoretical analysis, the performance simulation of the DFIG for the nonlinear crowbar circuit is conducted with a sag depth of 0.2 p.u.. The generator parameters are given in Appendix B. According to (24) and the equivalent conversion between the linear and nonlinear circuits, the optimal resistance applied in the nonlinear circuit to realize the fastest attenuation rate can be expressed as:

$$R_{c\_nonlinear\_opt}=3.3\times\sqrt{3v_1^2+3w_1^2}=5.9(\Omega) \quad (28)$$

For comparing the calculated result with those of the simulation and the experiment, the crowbar resistors applied in this paper are uniform. Due to the limitations imposed by the experimental condition in the laboratory, a $0.25\,\Omega$ power resister which approximates the calculation result of (28) is applied instead. This substitution leads to a larger time constant $-1/\mathrm{Re}(a_3)$. Through an equivalent conversion from a linear to a nonlinear circuit and a winding conversion, $R_r^{'}$ can be calculated including the rotor resistor and the crowbar resister:

$$R_r^{'}=0.3226+0.25\times(1/\sqrt{3v_1^2+3w_1^2})\times(1/k^2)=0.3383(\Omega) \quad (29)$$

As a result, $R_{c\_nonlinear}^{'}$ is set to $0.25\times(1/k^2)\Omega$ in the MATLAB/SIMPOWER model of a nonlinear crowbar circuit. The attenuation ratio in 40ms is $\sigma=e^{\mathrm{Re}(a_3)|_{R_r^{'}=0.3383}\times 0.04}=27.36\%$ if $R_r^{'}=0.3383\Omega$, which is acceptable when compared with σ_{opt}. The attenuation time constants of the transient components are equal in the positive and negative sequence as concluded from (9), (10), (16) and (17). Without losing generality and for simplifying the model, simulations and experiments are carried out under the symmetrical fault condition.

A grid fault occurred at t=0.402s when the space vector of the grid voltage was $690e^{j(\frac{-3\pi}{10})}$ and grid voltage space vector was $0.2\times 690e^{j[\omega_1(t-0.402)-\frac{3\pi}{10}+\frac{\pi}{12}]}$ with a phase jump after the occurrence of a sag. The electrical angular speed of the rotor is set to be constant which is $80\pi(rad/s)$, viz. , the mechanical rotational speed is $126(rad/s)$.

Fig. 3 and Fig. 4 show a comparison of the simulated and calculated transient stator current which are i_{sim} and i_{cal} in the stator stationary reference frame assuming that the crowbar resistor is fired permanently once a grid fault occurs. The horizontal axes indicate the time t in both the calculation and the simulation. For lining up the time bases of the simulated and calculated values, the calculated value is set to be zero before a fault occurs.

Fig. 5 and Fig. 6 give the simulated and calculated transient rotor currents which are i_{sim} and i_{cal} in the stator reference

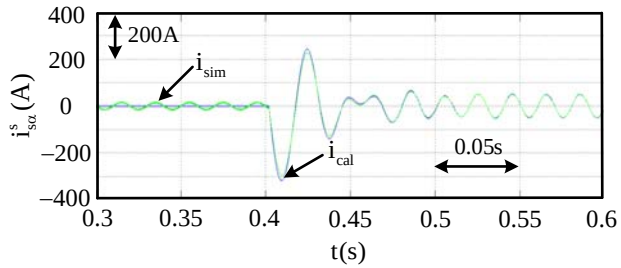

Fig. 3. Simulated and calculated stator current in α axis of stator.

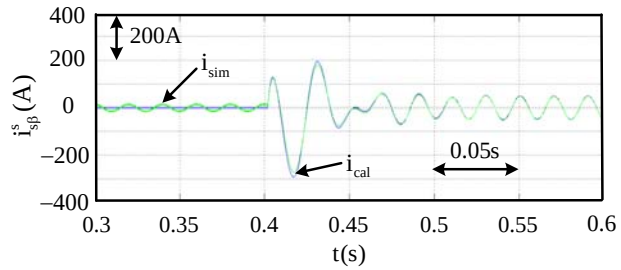

Fig. 4. Simulated and calculated stator current in β axis of stator.

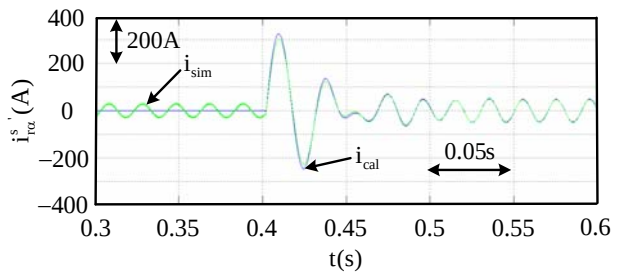

Fig. 5. Simulated and calculated rotor current in α axis of stator.

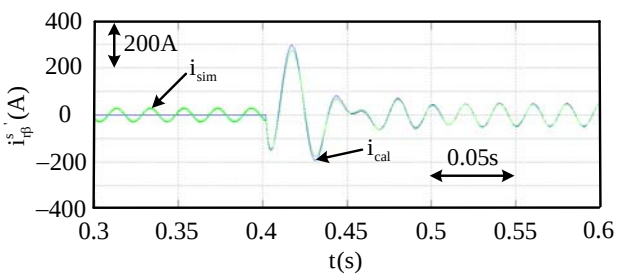

Fig. 6. Simulated and calculated rotor current in β axis of stator.

frame.

As shown by Fig. 5 and Fig. 6, the calculated current of the linear circuit is almost identical to the simulated result carried out using the nonlinear crowbar model. The extra harmonic current due to nonlinear rectifying has little influence on the results.

The amplitude of the crowbar current and the line voltage at the rotor side converter should be guaranteed to be within the safe operating area for the generator, the crowbar and the rotor side converter. The above result shows that $|i^{s'}_{r\alpha}| \le 330A$ and $|i^{s'}_{r\beta}| \le 300A$. When the crowbar is fired, it can be calculated that:

$$\left|\vec{i}^{s}_{r}\right| = \left|\vec{i}^{s'}_{r}\right| / k \le \sqrt{\max|i^{s'}_{r\alpha}|^2 + \max|i^{s'}_{r\beta}|^2} / k = 150(A) \quad (30)$$

$$i_{crowbar\_\max} = \max\{\max|i_{crowbar\_a}|, \max|i_{crowbar\_b}|, \max|i_{crowbar\_c}|\} \quad (31)$$

Thereafter, $i_{crowbar\_\max}$ can be calculated by (30) and (31) with a range of $i_{crowbar\_\max} \le 366A$. Then the maximum value of the line voltage at the rotor side U_{line_max} is given by:

$$U_{line\_max} \le i_{crowbar\_\max} \times R_{c\_nonlinear} \times \sqrt{3} << U_{dc} = 1100V \quad (32)$$

The above analysis shows that the rotor side converter is bypassed by the crowbar. However, the rotor current impact is inevitable.

VI. Experimental Validation of the Proposed Calculation Method

In order to validate the analysis in the previous sections, tests are performed using the system shown in Fig. 7(a), while the theory of equivalent conversion between the linear and nonlinear crowbar is illustrated by Fig. 7(b). Pictures of experimental setup are shown in Fig. 7(c)-(e). The experimental system includes the following items:

(1) The parameters of a DFIG are listed in Appendix B.

(2) A 2MW voltage source converter (VSC) operating at 2kHz switching frequency and a RLC filter are connected to the stator of the DFIG, which is controlled to simulate a voltage sag of the grid.

(3) A wind turbine simulation system that outputs a signal of the rotation speed and a DC motor is applied as the actuating mechanism.

(4) The resistance of $R^{'}_{c\_nonlinear}$ which is equal to 0.0157Ω calculated by $0.25\Omega * (1/\sqrt{3v_1^2 + 3w_1^2}) * (1/k^2)$ is converted to $R_{c\_nonlinear} = 0.25\Omega$ and is used in the nonlinear crowbar circuit.

The identities of the calculated and the experimental transient current can be made out from Fig. 8 and Fig. 10. The time period while the crowbar is being fired is expressed by the rectangular box in Fig. 9 and Fig. 11. After the crowbar is switched off, the rotor current controlled by the RSC is resumed to supply reactive current (the RMS value of the phase current is equal to 35A) at the stator side.

Fig. 9 and Fig. 11 show waveforms obtained by scope capture. Due to the scope design of the waveform recording function, the sign of the time axis is shown as negative in this time span. For lining up the time bases of the experimental and calculated values, the divisions of the horizontal axes in Fig. 8 and Fig. 10 are specified corresponding to those obtained by the scope capture, hence t_{sag} is equal to -5.4225s. As can be seen from Fig. 12, the rotation speed of the DFIG changes in the experiment. The speed (ω_r / p_n) is 126rad/s before a grid

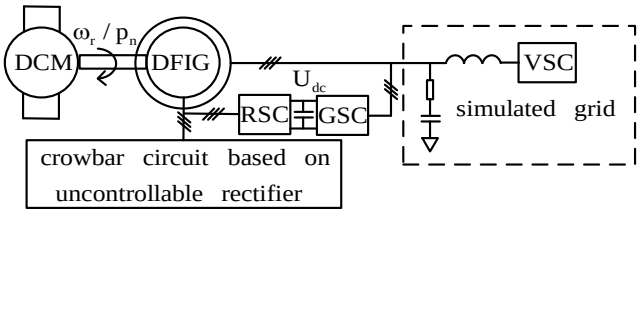

(a)

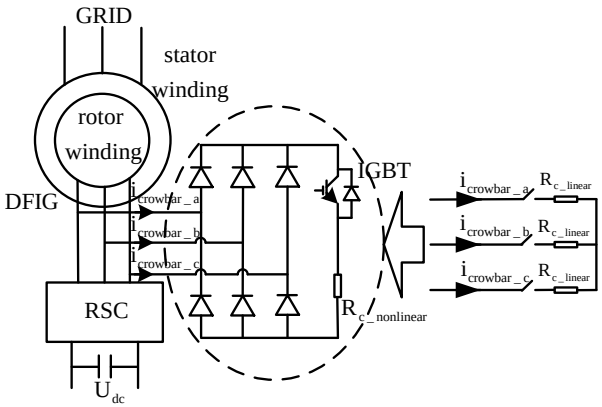

(b)

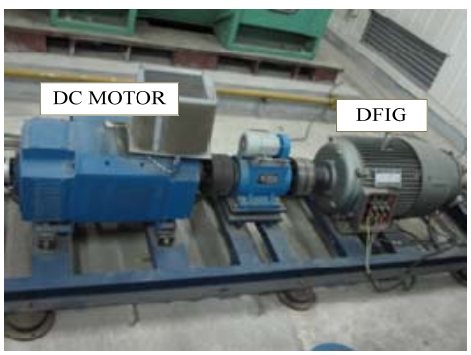

(c)

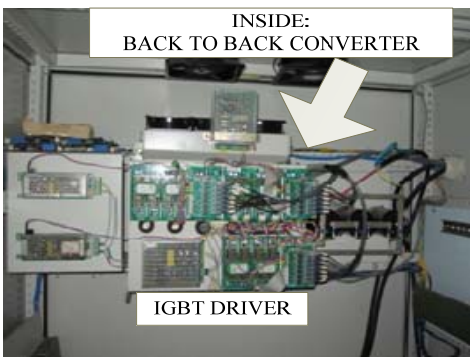

(d)

(e)

Fig. 7. Experimental system: (a) 30kW test rig, (b) Equivalent conversion between linear and nonlinear crowbar, (c) The picture of the 30kW driving setup, (d) The power circuit of the converter for DFIG, (e) The 2MW converter for simulating the grid.

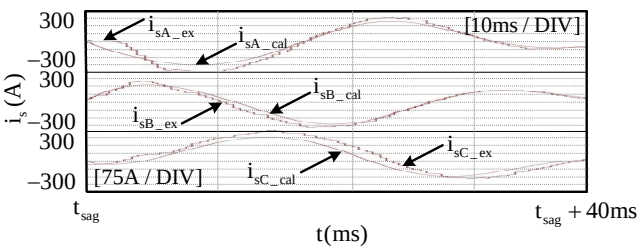

Fig. 8. Calculated and experimental stator current when crowbar is turned on.

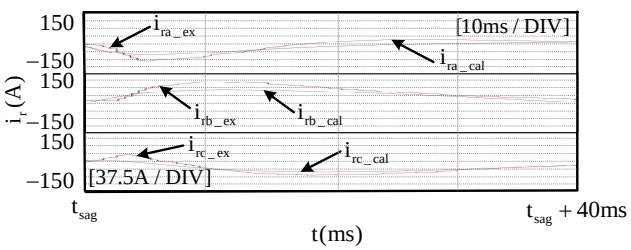

Fig. 10. Calculated and experimental rotor current when crowbar is turned on.

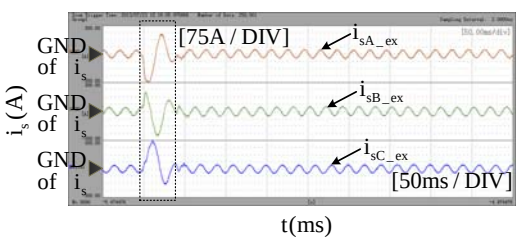

Fig. 9. Experimental stator current during crowbar is operating and the compensated reactive current of stator.

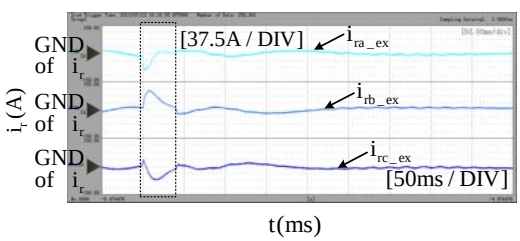

Fig. 11. Experimental rotor current during crowbar is operating and the reactive AC excitation after the control of RSC is resumed.

fault. The time interval of the crowbar being fired is given in the rectangular box of Fig. 12, during which time the speed variation is small. The calculated values given by Fig. 8 and Fig. 10 are provided and ω_r / p_n is approximately equal to 126rad/s. This waveform is exported from the RAM on the DSP board. For lining up the time base of Fig. 12 and that of the scope capture, the division of the horizontal axis is specified corresponding to that obtained by the scope capture.

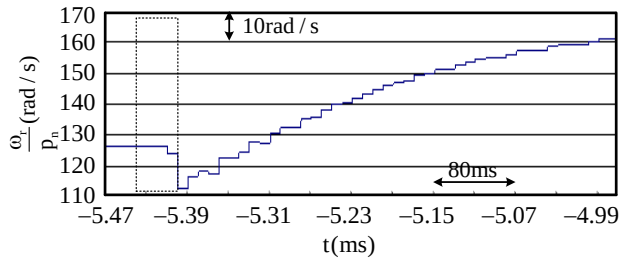

Fig. 12. Rotor speed of the DFIG.

In the experiment, the steady-state control algorithm realizes the controllability of the rotor current after the crowbar is switched off. The waves indicate the correctness of the proposed calculation method and the accuracy of the attenuating characteristics figured out.

VII. Conclusions

The proposed approach is worthwhile in three aspects: a) the DFIG's influence on the grid of the transient current during LVRT is determined; b) the selection of the crowbar resistance is realized by a mathematical method; c) a theoretical basis is proposed for optimizing the parameters of the DFIG to improve the performance of LVRT.

Simulation and experimental studies on a 30kW wind power DFIG system are carried out to validate the proposed theoretical method. As a result, the following conclusions can be drawn:

1) On the basis of the linear resolution, the crowbar resistance can be selected and converted to a nonlinear circuit with the coefficient $\sqrt{3v_1^2+3w_1^2}$.

2) The time constant of the exponential attenuation of transient components depends on the parameters of the DFIG, the rotating speed and the crowbar resistance, while being irrelevant to the depth of the voltage sag and the angle of the phase jump.

3) When the crowbar resistor is set to guarantee the attenuation rate if the DFIG is running with the highest positive slip, the crowbar circuit insures a higher attenuation rate of the transient components at a higher rotating speed.

4) The maximum negative real part of the exponents that is in the expressions of the transient components is pivotal for deciding the attenuation rate.

5) The resolution of the time constant realizes the selection of the crowbar resistance and the duration time set up of the crowbar protection, which reserves a response time for the reactive power support.

6) The crowbar resistor can be selected both to set the attenuation rate and to decrease the transient current of the DFIG, and the latter will be further studied in another paper.

7) Although it has been proven in this paper that $U_{line\_max} << U_{dc}$, U_{line_max} depends on the conditions before a sag, the asymmetrical characteristics of the voltage sag, the depth of the voltage sag and the parameters of the generator. The possibility that the design of the crowbar would be unable to insure $U_{line\_max} < U_{dc}$ and a proper attenuation rate simultaneously will be researched in a future work.

Appendix A

This appendix gives the transient rotor current expression of the zero-state response (A1) and the zero-input response (A2) in the frequency domain.

$$\boldsymbol{I}_{r1}^{s'} = -\frac{L_m'(s-j\omega_r)(s+j\omega_1)|U_{spm}|e^{j\theta_{sp0}}}{(s^2+\omega_1^2)A_1} - \frac{L_m'(s-j\omega_r)(s-j\omega_1)|U_{snm}|e^{j\theta_{sn0}}}{(s^2+\omega_1^2)A_1} \quad \text{(A1)}$$

$$\boldsymbol{I}_{r2}^{s'} = \frac{A_1\psi_r^{s'}(t_0) - (s-j\omega_r)L_m'[B_1\psi_s^{s}(t_0) - sL_m'\psi_r^{s'}(t_0)]}{A_1B_1} \quad \text{(A2)}$$

Appendix B

TABLE BI

DFIG Parameters Used in Simulation and Experiment

Parameters	Value
Rated power(kW)	30
Rated stator voltage(V)	690
Rated frequency(Hz)	50
Rated stator current(A)	32
Rated rotor current(A)	12
Winding connection(stator/rotor)	Y/Y
Number of pole-pairs	2
Range of speed(r/min)	1200-1800
Winding conversion coefficient (k)	2.97
Resistance of a stator winding(Ω)	0.8784
Self-inductance of a stator winding(H)	0.09525
Mutual inductance(H)	0.2607
Resistance of a rotor winding(Ω)	2.8456
Resistance of a rotor winding after winding conversion(Ω)	0.3226
Self-inductance of a rotor winding (H)	0.8035

Acknowledgment

This work was supported and funded by the grants of Natural Science Foundation of Jiangsu Province, China(BK20141095), Natural Science Foundation of China(51277025), Natural Science Foundation of China (50977010) and Scientific Research Foundation for High-level Introduction of Talent(YKJ201521), Nanjing Institute of Technology, China.

References

[1] Y. He and P. Zhou, "Overview of the low voltage ride-through technology for variable speed constant

frequency doubly fed wind power generation systems," *Transactions of China Electrotechnical Society*, Vol. 24, No. 9, pp. 140-146, Sep. 2009.
[2] J. Morren, and S. W. H. De Haan, "Short-circuit current of wind turbines with doubly-fed induction generator," *IEEE Trans. Energy Convers.*, Vol. 22, No.1, pp. 174-180, Mar. 2007.
[3] J. Zhai, B. Zhang, K. Wang, and W. Shao, "Three-phase symmetrical short circuit current characteristic analysis of doubly fed induction generator with crowbar protection," *IEEE PES Innovative Smart Grid Technologies*, pp. 1-5, May 2012.
[4] H. Soliman, M. I. Marei, R. M. El-Sharkawy, K. M. El-Bahrawy, "Analysis of the dynamic behavior of a DFIG during grid disturbances using active crowbar protection," in *12th International Conference on Environment and Electrical Engineering (EEEIC)*, pp. 160-163, May 2013.
[5] M. Ding, T. Hu, P. Han, and D. Wang, "Analysis of low voltage ride through ability of variable speed constant frequency wind turbine based on crowbar protection," in *Asia-Pacific Power and Energy Engineering Conference (APPEEC)*, pp. 1-5, Mar. 2012.
[6] Z. Zheng, G. Yang, and H. Geng, "Short circuit current analysis of DFIG-type WG with crowbar protection under grid fault," in *IEEE International Symposium on Industrial Electronics (ISIE)*, pp. 1072-1079, May 2012.
[7] Y. Ren and W. Zhang, "A novel control strategy of an active crowbar for DFIG-based wind turbine during grid fault," in *IEEE International Electric Machines & Drives Conference (IEMDC)*, pp. 1137-1142, May 2011.
[8] L. Zhang, X. Jin, and L. Zhan, "A novel LVRT control strategy of DFIG based rotor active crowbar," in *Asia-Pacific Power and Energy Engineering Conference (APPEEC)*, pp. 1-6, Mar. 2011.
[9] M. Wang, W. Xu, H. Jia, and X. Yu, "A novel method to optimizing the active crowbar resistance for low voltage ride through operation of doubly-fed induction generator based on wind energy," in *IEEE International Symposium on Industrial Electronics (ISIE)*, pp. 957-962, May 2012.
[10] A. Zohoori, J. S. Moghani, S. H. Fathi, and V. Mortezapour, "An optimized crowbar for DFIG with AHP algorithm under single phase fault," in *10th International Conference on Environment and Electrical Engineering (EEEIC)*, pp. 1-4, May 2011.
[11] J. Lopez, E. Gubia, P. Sanchis, and X. Roboam, "Wind turbine based on doubly-fed induction generator under asymmetrical voltage dips," *IEEE Trans. Energy Convers.*, Vol. 23, No. 1, pp. 321-330, Mar. 2008.
[12] G. Pannell, D. J. Atkinson, and B. Zahawi, "Analytical study of grid-fault response of wind turbine doubly fed induction generator," *IEEE Trans. Energy Convers.*, Vol. 25, No. 4, pp. 1081-1091, Dec. 2010.
[13] L. Zhang, X. Cai, and J. Guo. "Dynamic responses of DFIG fault currents under constant AC excitation condition," in *Asia-Pacific Power and Energy Engineering Conference*, pp. 1-4, Mar. 2009.
[14] Z. Wu, G. Wang, H. Li, T. Ding, and X. Gao, "Fault current contribution of DFIG under unsymmetrical fault," in *4th International Conference on Electric Utility Deregulation and Restructuring and Power Technologies (DRPT)*, pp. 1687-1692, Jul. 2011.
[15] X. Gao, G. Wang, Z. Wu, and H. Li, "Fault current contribution of doubly fed induction generator wind turbines under different control strategies," in *International Conference on Advanced Power System Automation and Protection (APAP)*, Vol. 2, pp. 1209-1214, Oct. 2011.
[16] H. L. Zhou, G. Yang, and D. Y. Li, "Short circuit current analysis of DFIG wind turbine with crowbar protection," in *International Conference on Electric Machine and Systems (ICEMS)*, pp. 1-6, Nov. 2009.
[17] Y. Tang, Y. Zhang, and Y. Fan, *Dynamic analysis of AC machine*, Chapter. 3, pp. 67-75, China Machine Press, 2004.

Hao Luo received his B.Eng. degree in Electronic Engineering from the South-Central University for Nationalities, Wuhan, China, in 2000; and his M.Eng. and Ph.D. degrees in Electrical Engineering from Southeast University, Nanjing, China, in 2008 and 2015, respectively. From 2000 to 2015, he was a R&D Engineer in the Nanjing Electric Power Automation Equipment General Factory and the Guodian Nanjing Automation Co., Ltd. (SAC), Nanjing, China, where he was involved in the development of frequency converters, photovoltaic inverters and wind power converters. From 2011 to 2015, he was the Chief Engineer and Assistant Chief Engineer of the Wind Power Automation Technology Co., Ltd., SAC and the New Energy Technology Co., Ltd., SAC, respectively. In 2015, he joined the School of Electric Power Engineering, Nanjing Institute of Technology, Nanjing, China. His current research interests include the design and control of high efficiency wind power generators, electric vehicles drives, and grid connected converters for renewable energy generation.

Mingyao Lin received B.Eng., M.S. and Ph.D. degrees in Electrical Engineering from Southeast University, Nanjing, China, in 1982, 1985 and 1995, respectively. In 1985, he joined the School of Electrical Engineering, Southeast University. Since 2004, he has been a Professor of Electrical Machines and Control Systems in the School of Electrical Engineering, Southeast University, where he was also the Director of the Department of Electrical Machines and Drives. In 2002, he was a Visiting Scholar at Fachhochschule Esslingen, Hochschule für Technik (FHTE), Esslingen University of Applied Sciences, Esslingen am Neckar, Germany. He has published more than 150 technical papers and holds 32 patents in his areas of interest. His current research interests include the design and control of high efficiency permanent magnet machines, electric vehicle drives, and renewable energy generation technology.

Yang Cao received his B.Eng. degree in Electrical Machines and Control Systems from Shenyang University of Technology, Shenyang, China, in 2002. He is presently working towards his M.Eng. degree in Electrical Engineering from Hohai University, Nanjing, China. From 2002 to 2015, he was a R&D Engineer in the Nanjing Electric Power Automation Equipment General Factory and the Guodian Nanjing Automation Co., Ltd. (SAC), Nanjing, China, where he was involved in the development of linear motor drivers, frequency converters, photovoltaic inverters and wind power converters. Since 2015, has been a Senior Designer in the Nanjing Sciyon Automation Group Co. Ltd., Nanjing, China, where he is involved in the development of grid connected converts for renewable energy.

Wei Guo received his B.Eng. degree in Electrical Engineering from Southwest Jiaotong University, Chengdu, China, in 2006; and his M.S. degree in Electrical Engineering from Southeast University, Nanjing, China, in 2009. In 2009, he joined the Guodian Nanjing Automation Co., Ltd. (SAC), Nanjing, China, where he is involved in the development of wind power converters.

Li Hao received her Ph.D. degree in Electrical Engineering from Southeast University, Nanjing, China, in 2015. She has published more than 11 technical papers and holds 2 patents in her areas of interest. Her current research interests include the design and control of high efficiency permanent magnet machines and electric vehicles drives.

Peng Wang has been working towards his B. Eng. degree in the School of Electric Power Engineering, Nanjing Institute of Technology, Nanjing, China, since 2014. His current research interests include motor modeling based on Matlab/Simulink and embedded systems development.